Absorption Spectroscopy of Single Optically Trapped Gold Nanorods

ARTICLE *in* NANO LETTERS · OCTOBER 2015

Impact Factor: 13.59 · DOI: 10.1021/acs.nanolett.5b03833

NANO LETTERS

Letter

pubs.acs.org/NanoLett

Absorption Spectroscopy of Single Optically Trapped Gold Nanorods

Zhongming Li, Weizhi Mao, Mary Sajini Devadas, and Gregory V. Hartland*

Department of Chemistry and Biochemistry, University of Notre Dame, 251 Nieuwland Science Hall, Notre Dame, Indiana 46556-5670, United States

Supporting Information

ABSTRACT: Extinction spectra of single gold nanorods optically trapped in water were measured by spatial modulation spectroscopy. Comparison of the extinction cross sections and resonance frequencies to finite element calculations allows us to determine the dimensions of the nanorod and estimate the contribution of radiation damping to the LSPR line width. Subtracting the radiation damping and bulk contributions from the measured line widths yields the electron−surface scattering contribution. The results show that the surfactant coating for the nanorods causes large electron−surface scattering effects with significant particle-to-particle variations. These effects are more pronounced than those seen for substrate-supported particles in previous single particle studies. Indeed, the measured line widths are only slightly narrower than that of the ensemble spectrum. These results show the importance of removing surfactant for sensing applications of these materials.

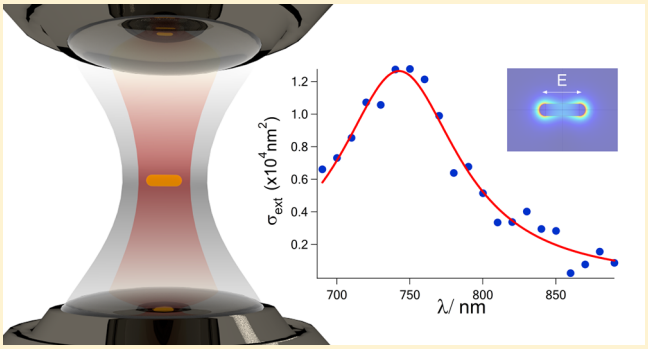

KEYWORDS: *Spatial modulation spectroscopy, electron−surface scattering, gold nanorods, single particle, optical trapping*

Gold nanoparticles have attracted considerable research interest for the past decade, mostly inspired by the properties of their localized surface plasmon resonances (LSPRs).[1−6] The LSPR is a collective oscillation of the conduction electrons that gives rise to an enhanced optical response in the visible to near-infrared region.[1−6] Among the different shapes of gold nanoparticles, gold nanorods stand out as a particularly interesting case due to the tunability and the frequency range of their LSPRs.[6−9] Gold nanorods have two LSPR bands: a longitudinal band, corresponding to oscillation of the electrons along the major axis of the nanorod, and a transverse band resulting from electron oscillation across the nanorod.[6−13] The position of the longitudinal band depends on a variety of parameters, such as the aspect ratio, end-cap shape, volume, attached ligands, and local environment.[6−13] This resonance occurs in the near-IR region, coinciding with the biological "optical window".[14] Because of this, gold nanorods have found extensive use in biomolecule sensing, imaging, and photothermal therapy.[8,12−17]

In addition to their technological applications, the spectroscopy of gold nanorods is also of current interest in particular the LSPR line width.[18,19] The line width sets the enhancement of the optical response and the concomitant local field. Several mechanisms contribute to the LSPR line width: bulk damping (which includes electron−phonon scattering $\Gamma_{e\text{-}ph}$ and electron−electron scattering $\Gamma_{e\text{-}e}$), electron−surface scattering (Γ_{surf}), and radiation damping (Γ_{rad}).[18−20] Traditional ensemble measurements usually overestimate the plasmon line width because of inhomogeneous broadening, a problem that can be overcome by recording spectra of single particles using either Rayleigh scattering or optical absorption techniques.[21−30]

Previous single particle studies of the LPSR line width were performed with the particle on a supporting substrate.[18,19,21−29] The presence of the substrate shifts the LSPR to longer wavelengths and complicates modeling of the optical response of the nanoparticle.[28] The substrate can even create new features in the spectrum.[22] In addition, for most applications in biology and catalysis the nanorods are in a homogeneous liquid (usually aqueous) environment.[6−9,14−17] For these reasons, a quantitative study of the LSPR of single gold nanorods in aqueous solution is highly desirable. Here we present the first direct absorption spectroscopy study on single gold nanorods in water. Optical trapping is utilized to immobilize the gold nanorods,[31−34] and spatial modulation spectroscopy (SMS) is then implemented to record the extinction cross-section across the longitudinal LSPR band.[19,26−28,35] The spectral results are compared to finite element (FE) calculations to unravel the different contributions to the line width, which is the major focus of the study.

Commercially available CTAB-capped gold nanorods (Nano-Partz) were used in our experiments. Figure 1A shows a representative transmission electron microscopy (TEM) image of the sample. The nanorods appear as hemisphere capped cylinders with an average width of 21 ± 2 nm and length of 79 ± 11 nm. For optical measurements, the nanorod solution was

Received: September 21, 2015
Revised: October 19, 2015

DOI: 10.1021/acs.nanolett.5b03833
Nano Lett. XXXX, XXX, XXX−XXX

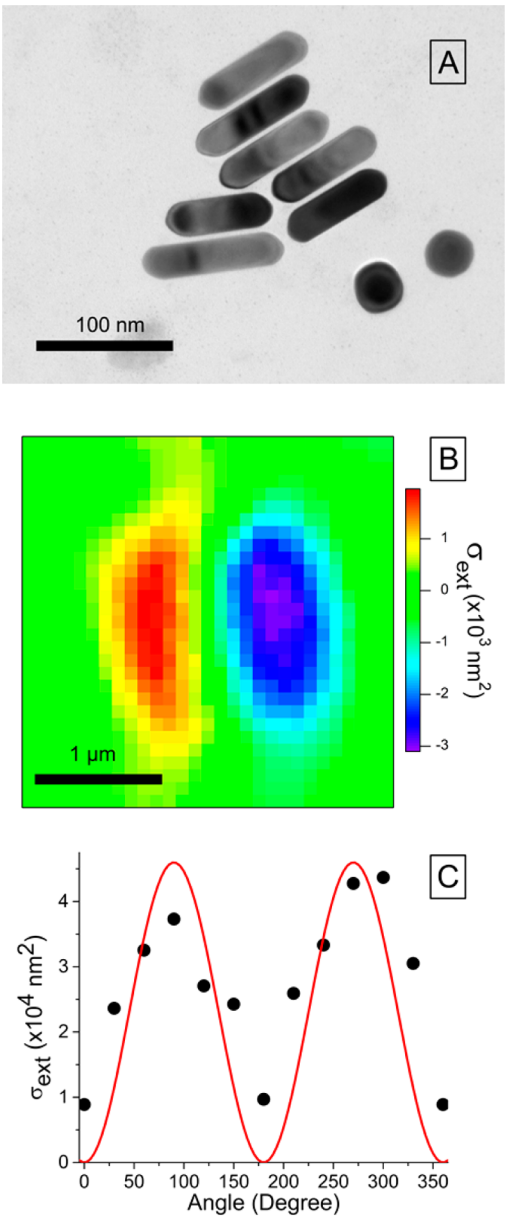

Figure 1. (A) TEM image of the gold nanorod sample. (B) Contour plot of the 1*f* SMS signal for an optically trapped gold nanorod recorded at 780 nm. (C) Plot of the polarization dependence of the extinction cross-section (again, measured at 780 nm).

greatly diluted (about 500 times) to produce a stable, single-particle optical trap. The optical trap was constructed by tightly focusing a linearly polarized near-infrared (1064 nm) laser with a high numerical aperture objective. A colinear tunable Ti:sapphire laser (680−900 nm) was used to interrogate the trapped particles. A galvo-scanning mirror system was integrated into the optical path of the T:Sapphire laser to allow both raster scanning and spatial modulation of the probe beam.[35,36] All the SMS data in this study was collected at the fundamental (1*f*) of the spatial modulation frequency. The polarizations of the trap and probe laser were set to be parallel for the majority of the experiments. This maximizes the signal for the longitudinal plasmon resonance; optically trapped nanorods are aligned with the polarization of the trapping laser[31−33] and the maximum extinction for the longitudinal LSPR occurs when the probe laser is parallel to the major axis of the nanorod.[1,10,11] More details about the experimental setup are given in the Supporting Information.

Figure 1B shows a 1*f* SMS image of a single optically trapped gold nanorod. In SMS, the relative position of the laser beam relative to the particle is modulated by a few hundred nanometers.[19] The change in transmitted power detected at the fundamental (1*f*) of the modulation frequency is

$$\left(\frac{\Delta P}{P_0}\right)_{1f} = \frac{8}{\pi}\frac{\sigma_{ext}\delta}{w_0^4}x\,\exp\left(-\frac{2(x^2+y^2)}{w_0^2}\right) \quad (1)$$

where δ is the modulation distance (0.16 μm), w_0 is the spot size, and σ_{ext} is the extinction cross-section.[19] Using this expression to analyze the SMS image in Figure 1B yields an extinction cross-section of 29 600 ± 2400 nm^2. Figure 1C shows that rotating the polarization of the probe light changes the amplitude of the extinction cross-section, as expected for the longitudinal LSPR of single gold nanorods.[28,29,37] Repeating SMS measurement at different wavelengths allows us to measure the extinction spectrum of the nanorod.

We measured spectra for eight optically trapped single gold nanorods. Three examples are displayed in Figure 2, together

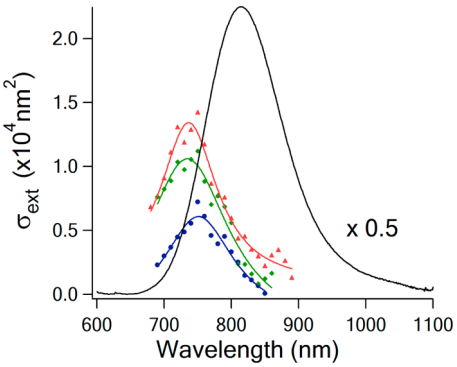

Figure 2. Extinction cross-section (σ_{ext}) spectra of three optically trapped gold nanorods (triangle, square, and dot). The lines show fits to the data using a quasi-Lorentz profile. The solid black line is the ensemble UV−vis spectrum, scaled to match the extinction cross-section for the average sized nanorod in the sample.

with the ensemble UV−vis spectrum of the sample. As expected, the LSPR spectra for the single nanorods occur at different frequencies due to structural differences between the particles. The spectra were fitted to a quasi-Lorentzian function[19,27,29]

$$\sigma_{ext} = \Xi\frac{\frac{\Gamma}{2\pi}}{(\omega-\Omega_R)^2+\left(\frac{\Gamma}{2}\right)^2} \quad (2)$$

where Ω_R is the center frequency, Γ is the line width, and Ξ is the integrated oscillator strength. The values of Ω_R, Γ, and Ξ determined for the different nanorods are presented in Table S2 of the Supporting Information.

The parameters Ω_R and Ξ depend on the dimensions of the nanorods and in principle can be used to determine the aspect ratio and volume. However, the relationship between Ω_R and Ξ and the dimensions is complicated, because the nanorods in our experiments are large enough to experience retardation effects.[38] This was confirmed by FE calculations that show that for a given aspect ratio increasing the volume redshifts the

DOI: 10.1021/acs.nanolett.5b03833
Nano Lett. XXXX, XXX, XXX−XXX

extinction spectrum (see Figure S3 and Table S1 in the Supporting Information).

In order to determine the dimensions of the nanorods in our experiments, FE calculations were used to ascertain how Ω_R and Ξ change with volume for a series of different aspect ratios. In these calculations, the nanorods were modeled as hemisphere-capped cylinders, which is consistent with the TEM observations. The dielectric constant of bulk gold was used[39] without corrections for electron−surface scattering.[24] This data is presented in Figure 3 as a surface plot, where volume is

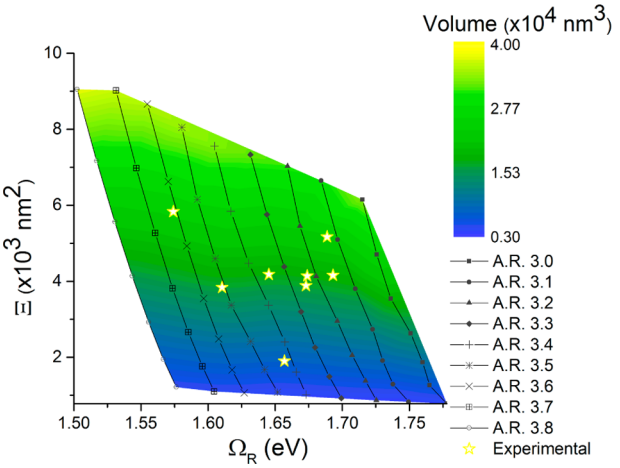

Figure 3. Three-dimensional surface plot of volume versus resonance frequency Ω_R and Ξ. The lines show results from finite element simulations for specific aspect ratios. The surface is generated by interpolating between the different lines.

treated as the dependent variable and Ω_R and Ξ as the independent variables. This surface is made up of a series of lines corresponding to different aspect ratios, which are essentially parallel to each other (see Figure 3). The volume and aspect ratio can be estimated from this plot by simply reading across from the measured values of Ω_R and Ξ and interpolating between the calculated lines. The values obtained for the different nanorods are included in Table S2 of the Supporting Information.

A plot of the line width from the experimental measurements versus the volume determined from Ω_R and Ξ is presented in Figure 4. The total line width has contributions from bulk damping (electron−phonon and electron−electron scattering), electron−surface scattering, and radiation damping: $\Gamma = \Gamma_{bulk} + \Gamma_{surf} + \Gamma_{rad}$.[18−20,23,29] The data in Figure 4 can be used to determine the electron−surface scattering component by subtracting the bulk and radiation damping contributions. For the bulk contribution, we note that at frequencies far away from interband transitions (which is the case for our measurement) Γ_{bulk} is independent of wavelength with a value of 73 meV at room temperature.[18−20,23,29] However, this quantity increases with temperature, primarily because of increased electron−phonon scattering,[40−42] and the nanorods in our experiments experience elevated lattice temperatures due to the trap laser. Orrit and co-workers determined a temperature increase with trap power of 0.9 K/mW for optically trapped nanorods with similar aspect ratios as those interrogated in our experiments.[31] Using this number gives a temperature increase of 126 ± 42 K for our experiments, which implies an estimated increase in Γ_{bulk} of 16 ± 5 meV, which is a relatively small effect.

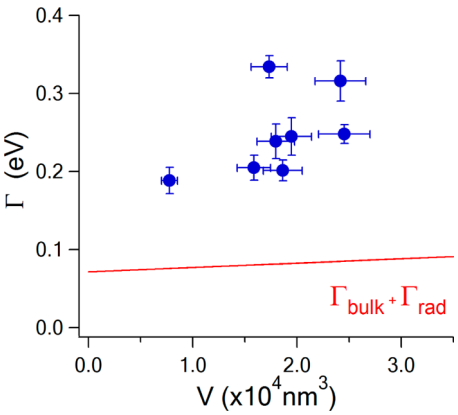

Figure 4. Total line widths measured from individual gold nanorods plotted against their estimated volumes. The solid red line shows the bulk and radiation damping contributions to the line width.

The radiation damping contribution to Γ is proportional to volume and, therefore, is different for the different nanorods in our experiments. This contribution is typically written as[21,23]

$$\Gamma_{rad} = 2\hbar\kappa V \tag{3}$$

where the proportionality constant κ depends on the details of the shape and material of the nano-object. Here we use FE simulations to estimate κ (see Figure S4 in the Supporting Information). The line widths of the longitudinal LSPRs in the simulated spectra were determined, and the radiation damping contributions were obtained by subtracting the bulk contribution from the total damping. This analysis yields a value of $2\hbar\kappa = 6.6 \times 10^{-7}$ eV·nm^{-3}, which is in good agreement with previous experimental measurements.[18,21,23] The solid line in Figure 4 shows the bulk and radiation damping ($\Gamma_{bulk} + \Gamma_{rad}$) contributions to the line width determined from our analysis. The difference between this line and the experimental measurements is the electron−surface scattering contribution.

Note that the values of σ_{ext} and, therefore, the experimentally determined volumes, are very sensitive to w_0. This parameter is not as well-known in our experiments compared to SMS measurements on substrate supported particles due to spherical aberrations in the optics[31,35,43] and because trapped particles are generally not located at the focus of the beams due to scattering forces.[44] The upshot is that our experimental volumes may be underestimated. However, as shown in Figure 4, radiation damping does not play a large role in the line width for this sample. Thus, the electron−surface scattering contributions determined from our analysis are not strongly affected by errors in w_0. In addition, fits to the SMS data yield similar values of w_0 as those obtained from the camera images (see the Supporting Information). This means that any errors in w_0 and, therefore, σ_{ext} are likely to be small.

Figure 5 shows the values of Γ_{surf} obtained by subtracting $\Gamma_{bulk} + \Gamma_{rad}$ from the experimental line widths plotted against the inverse effective path length $1/L_{eff}$ for the electrons. The effective path length is calculated as $L_{eff} = 4V/S$, where S is the surface area of the nanorod and V is the volume.[1,18,19,25] For a hemisphere-capped cylinder $L_{eff} = w(1 - w/3l)$, where w is the width and l is the total length. The shaded area in Figure 5 shows the electron−surface scattering contribution calculated from

DOI: 10.1021/acs.nanolett.5b03833
Nano Lett. XXXX, XXX, XXX−XXX

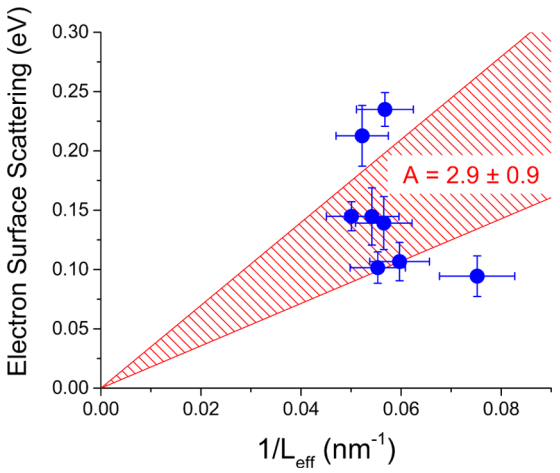

Figure 5. Contribution from electron−surface scattering to the line width plotted against the inverse of the effective path length (L_{eff}). The electron−surface scattering parameter determined by fitting data into eq 4 is $A = 2.9 \pm 0.9$ (error equals 95% confidence limit, represented as the shaded area in the figure).

$$\Gamma_{surf} = \frac{A \cdot \nu_F}{L_{eff}} \quad (4)$$

In this equation $\nu_F = 1.4 \times 10^6$ ms^{-1} is the Fermi velocity, and the proportionality constant $A = 2.9 \pm 0.9$ (error equals 95% confidence limits) was determined from the experimental data points.

The electron−surface scattering contributions to the line width and the corresponding value of A determined from our measurements are very scattered and are larger than previous studies of surfactant-coated gold nanorods immobilized on a substrate.[21,23,27] Specifically, our previous single particle Rayleigh scattering measurements gave a value of $A = 0.30 \pm 0.03$ for CTAB-coated nanorods on a glass surface.[23,25] Recent SMS measurements by Vallee and co-workers for substrate-supported, surfactant-coated gold nanorods also showed electron−surface scattering effects approximately 2× smaller than those for the present experiments (line width contributions on the order of 100 meV, rather than the 100−200 meV values seen here).[27]

The larger line widths seen in the present experiments compared to previous single particle measurements[23,27] are attributed to the surfactant layer surrounding the nanorods. Recent SMS measurements on substrate-supported particles have shown that silica-coated nanorods have smaller line widths than surfactant-coated particles,[27,29] implying that removing the surfactant coating (CTAB) reduces the line width. We expect that the nanorods in our experiments will have more CTAB than those in refs 23 and 27; no effort was made to remove the CTAB in our trapping measurements, whereas several dilution/centrifugation steps were used for the substrate-supported experiments. One could also speculate that heating from the trap laser disorders the surfactant layer and that this also contributes to the increased line width. However, it is not clear what the mechanism would be for this effect. These results show that it is crucial to remove CTAB from the surface of the nanorods for experiments where the shift in the plasmon resonance is used for sensing.[3,6,9,12,22] The sensitivity of these types of measurements is determined by the size of the shift divided by the line width, which means that samples with narrow resonances are highly desirable.[45]

In conclusion, we have reported the first absorption spectroscopy study of single, optically trapped gold nanorods. Our combination of optical trapping and SMS provides direct extinction cross-section information for gold nanorods in a homogeneous aqueous environment. The volumes and aspect ratios of the nanorods were determined by comparison to finite element calculations, allowing a comprehensive analysis of the different dephasing mechanisms for the plasmon resonance. The results show that the nanorods suffer significant electron−surface scattering effects, larger than those previously seen for substrate-supported nanorods. These results have important implications for sensing applications where the shift in the plasmon resonance of the nanorods is used to indicate a binding event.

■ ASSOCIATED CONTENT

Supporting Information

The Supporting Information is available free of charge on the ACS Publications website at DOI: 10.1021/acs.nanolett.5b03833.

Supporting Information available for this paper includes details of the experimental system and the finite element simulations; tabulated experimental and calculated frequencies, line widths, and total cross sections; experimental spectra; and sample size distribution information. (PDF)

■ AUTHOR INFORMATION

Corresponding Author

*E-mail ghartlan@nd.edu.

Notes

The authors declare no competing financial interest.

■ ACKNOWLEDGMENTS

This work was supported by the United States National Science Foundation (CHE-1110560), and the Office of Naval Research (Award No. N00014-12-1-1030).

■ REFERENCES

(1) Kelly, K. L.; Coronado, E.; Zhao, L. L.; Schatz, G. C. The optical properties of metal nanoparticles: The influence of size, shape, and dielectric environment. *J. Phys. Chem. B* **2003**, *107*, 668−677.

(2) Lal, S.; Link, S.; Halas, N. J. Nano-optics from sensing to waveguiding. *Nat. Photonics* **2007**, *1*, 641−648.

(3) Willets, K. A.; Van Duyne, R. P. Localized surface plasmon resonance spectroscopy and sensing. *Annu. Rev. Phys. Chem.* **2007**, *58*, 267−297.

(4) Pelton, M.; Aizpurua, J.; Bryant, G. Metal-nanoparticle plasmonics. *Laser Photonics Rev.* **2008**, *2*, 136−159.

(5) Schwartzberg, A. M.; Zhang, J. Z. Novel optical properties and emerging applications of metal nanostructures. *J. Phys. Chem. C* **2008**, *112*, 10323−10337.

(6) Huang, X. H.; Neretina, S.; El-Sayed, M. A. Gold nanorods: From synthesis and properties to biological and biomedical applications. *Adv. Mater.* **2009**, *21*, 4880−4910.

(7) Jain, P. K.; Lee, K. S.; El-Sayed, I. H.; El-Sayed, M. A. Calculated absorption and scattering properties of gold nanoparticles of different size, shape, and composition: Applications in biological imaging and biomedicine. *J. Phys. Chem. B* **2006**, *110*, 7238−7248.

(8) Tong, L.; Wei, Q. S.; Wei, A.; Cheng, J. X. Gold nanorods as contrast agents for biological imaging: Optical properties, surface conjugation and photothermal effects. *Photochem. Photobiol.* **2009**, *85*, 21−32.

DOI: 10.1021/acs.nanolett.5b03833
Nano Lett. XXXX, XXX, XXX−XXX

(9) Becker, J.; Trugler, A.; Jakab, A.; Hohenester, U.; Sonnichsen, C. The optimal aspect ratio of gold nanorods for plasmonic bio-sensing. *Plasmonics* **2010**, *5*, 161−167.
(10) Murphy, C. J.; Sau, T. K.; Gole, A. M.; Orendorff, C. J.; Gao, J. X.; Gou, L.; Hunyadi, S. E.; Li, T. Anisotropic metal nanoparticles: Synthesis, assembly, and optical applications. *J. Phys. Chem. B* **2005**, *109*, 13857−13870.
(11) Perez-Juste, J.; Pastoriza-Santos, I.; Liz-Marzan, L. M.; Mulvaney, P. Gold nanorods: Synthesis, characterization and applications. *Coord. Chem. Rev.* **2005**, *249*, 1870−1901.
(12) Jain, P. K.; Huang, X. H.; El-Sayed, I. H.; El-Sayed, M. A. Noble metals on the nanoscale: Optical and photothermal properties and some applications in imaging, sensing, biology, and medicine. *Acc. Chem. Res.* **2008**, *41*, 1578−1586.
(13) Murphy, C. J.; Gole, A. M.; Stone, J. W.; Sisco, P. N.; Alkilany, A. M.; Goldsmith, E. C.; Baxter, S. C. Gold nanoparticles in biology: Beyond toxicity to cellular imaging. *Acc. Chem. Res.* **2008**, *41*, 1721−1730.
(14) Hu, M.; Chen, J.; Li, Z.-Y.; Au, L.; Hartland, G. V.; Li, X.; Marquez, M.; Xia, Y. Gold nanostructures: Engineering their plasmonic properties for biomedical applications. *Chem. Soc. Rev.* **2006**, *35*, 1084−1094.
(15) Huang, X. H.; El-Sayed, I. H.; Qian, W.; El-Sayed, M. A. Cancer cell imaging and photothermal therapy in the near-infrared region by using gold nanorods. *J. Am. Chem. Soc.* **2006**, *128*, 2115−2120.
(16) Dickerson, E. B.; Dreaden, E. C.; Huang, X. H.; El-Sayed, I. H.; Chu, H. H.; Pushpanketh, S.; McDonald, J. F.; El-Sayed, M. A. Gold nanorod assisted near-infrared plasmonic photothermal therapy (pptt) of squamous cell carcinoma in mice. *Cancer Lett.* **2008**, *269*, 57−66.
(17) Tucker-Schwartz, J. M.; Meyer, T. A.; Patil, C. A.; Duvall, C. L.; Skala, M. C. In vivo photothermal optical coherence tomography of gold nanorod contrast agents. *Biomed. Opt. Express* **2012**, *3*, 2881−2895.
(18) Hartland, G. V. Optical studies of dynamics in noble metal nanostructures. *Chem. Rev.* **2011**, *111*, 3858−3887.
(19) Crut, A.; Maioli, P.; Del Fatti, N.; Vallee, F. Optical absorption and scattering spectroscopies of single nano-objects. *Chem. Soc. Rev.* **2014**, *43*, 3921−3956.
(20) Kreibig, U.; Vollmer, M. *Optical properties of metal clusters*; Springer-Verlag: Berlin, 1995; Vol. *25*.
(21) Sonnichsen, C.; Franzl, T.; Wilk, T.; von Plessen, G.; Feldmann, J.; Wilson, O.; Mulvaney, P. Drastic reduction of plasmon damping in gold nanorods. *Phys. Rev. Lett.* **2002**, *88*, 077402.
(22) Sherry, L. J.; Chang, S. H.; Schatz, G. C.; Van Duyne, R. P.; Wiley, B. J.; Xia, Y. N. Localized surface plasmon resonance spectroscopy of single silver nanocubes. *Nano Lett.* **2005**, *5*, 2034−2038.
(23) Novo, C.; Gomez, D.; Perez-Juste, J.; Zhang, Z.; Petrova, H.; Reismann, M.; Mulvaney, P.; Hartland, G. V. Contributions from radiation damping and surface scattering to the linewidth of the longitudinal plasmon band of gold nanorods: A single particle study. *Phys. Chem. Chem. Phys.* **2006**, *8*, 3540−3546.
(24) Hu, M.; Chen, J.; Marquez, M.; Xia, Y.; Hartland, G. V. Correlated rayleigh scattering spectroscopy and scanning electron microscopy studies of Au-Ag bimetallic nanoboxes and nanocages. *J. Phys. Chem. C* **2007**, *111*, 12558−12565.
(25) Hu, M.; Novo, C.; Funston, A.; Wang, H.; Staleva, H.; Zou, S.; Mulvaney, P.; Xia, Y.; Hartland, G. V. Dark-field microscopy studies of single metal nanoparticles: Understanding the factors that influence the linewidth of the localized surface plasmon resonance. *J. Mater. Chem.* **2008**, *18*, 1949−1960.
(26) Baida, H.; Billaud, P.; Marhaba, S.; Christofilos, D.; Cottancin, E.; Crut, A.; Lerme, J.; Maioli, P.; Pellarin, M.; Broyer, M.; et al. Quantitative determination of the size dependence of surface plasmon resonance damping in single Ag@SiO_2 nanoparticles. *Nano Lett.* **2009**, *9*, 3463−3469.
(27) Lombardi, A.; Loumaigne, M.; Crut, A.; Maioli, P.; Del Fatti, N.; Vallee, F.; Spuch-Calvar, M.; Burgin, J.; Majimel, J.; Treguer-Delapierre, M. Surface plasmon resonance properties of single elongated nanoobjects: Gold nanobipyramids and nanorods. *Langmuir* **2012**, *28*, 9027−9033.
(28) Davletshin, Y. R.; Lombardi, A.; Fernanda Cardinal, M.; Juve, V.; Crut, A.; Maioli, P.; Liz-Marzan, L. M.; Vallee, F.; Del Fatti, N.; Kumaradas, J. C. A quantitative study of the environmental effects on the optical response of gold nanorods. *ACS Nano* **2012**, *6*, 8183−8193.
(29) Juve, V.; Fernanda Cardinal, M.; Lombardi, A.; Crut, A.; Maioli, P.; Perez-Juste, J.; Liz-Marzan, L. M.; Del Fatti, N.; Vallee, F. Size-dependent surface plasmon resonance broadening in nonspherical nanoparticles: Single gold nanorods. *Nano Lett.* **2013**, *13*, 2234−2240.
(30) Yorulmaz, M.; Nizzero, S.; Hoggard, A.; Wang, L. Y.; Cai, Y. Y.; Su, M. N.; Chang, W. S.; Link, S. Single-particle absorption spectroscopy by photothermal contrast. *Nano Lett.* **2015**, *15*, 3041−3047.
(31) Ruijgrok, P. V.; Verhart, N. R.; Zijlstra, P.; Tchebotareva, A. L.; Orrit, M. Brownian fluctuations and heating of an optically aligned gold nanorod. *Phys. Rev. Lett.* **2011**, *107*, 037401.
(32) Pelton, M.; Liu, M. Z.; Kim, H. Y.; Smith, G.; Guyot-Sionnest, P.; Scherer, N. E. Optical trapping and alignment of single gold nanorods by using plasmon resonances. *Opt. Lett.* **2006**, *31*, 2075−2077.
(33) Selhuber-Unkel, C.; Zins, I.; Schubert, O.; Sonnichsen, C.; Oddershede, L. B. Quantitative optical trapping of single gold nanorods. *Nano Lett.* **2008**, *8*, 2998−3003.
(34) Marago, O. M.; Jones, P. H.; Gucciardi, P. G.; Volpe, G.; Ferrari, A. C. Optical trapping and manipulation of nanostructures. *Nat. Nanotechnol.* **2013**, *8*, 807−819.
(35) Devadas, M. S.; Li, Z. M.; Hartland, G. V. Imaging and analysis of single optically trapped gold nanoparticles using spatial modulation spectroscopy. *J. Phys. Chem. Lett.* **2014**, *5*, 2910−2915.
(36) Devadas, M. S.; Li, Z.; Major, T. A.; Lo, S. S.; Havard, N.; Yu, K.; Johns, P.; Hartland, G. V. Detection of single gold nanoparticles using spatial modulation spectroscopy implemented with a galvo-scanning mirror system. *Appl. Opt.* **2013**, *52*, 7806−7811.
(37) Muskens, O. L.; Bachelier, G.; Del Fatti, N.; Vallee, F.; Brioude, A.; Jiang, X. C.; Pileni, M. P. Quantitative absorption spectroscopy of a single gold nanorod. *J. Phys. Chem. C* **2008**, *112*, 8917−8921.
(38) Slaughter, L. S.; Chang, W. S.; Swanglap, P.; Tcherniak, A.; Khanal, B. P.; Zubarev, E. R.; Link, S. Single-particle spectroscopy of gold nanorods beyond the quasi-static limit: Varying the width at constant aspect ratio. *J. Phys. Chem. C* **2010**, *114*, 4934−4938.
(39) Johnson, P. B.; Christy, R. W. Optical constants of the noble metals. *Phys. Rev. B* **1972**, *6*, 4370−4379.
(40) McKay, J. A.; Rayne, J. A. Temperature-dependence of infrared absorptivity of noble-metals. *Phys. Rev. B* **1976**, *13*, 673−685.
(41) Liu, M. Z.; Pelton, M.; Guyot-Sionnest, P. Reduced damping of surface plasmons at low temperatures. *Phys. Rev. B: Condens. Matter Mater. Phys.* **2009**, *79*, 035418.
(42) Konrad, A.; Wackenhut, F.; Hussels, M.; Meixner, A. J.; Brecht, M. Temperature dependent luminescence and dephasing of gold nanorods. *J. Phys. Chem. C* **2013**, *117*, 21476−21482.
(43) Hajizadeh, F.; Reihani, S. N. Optimized optical trapping of gold nanoparticles. *Opt. Express* **2010**, *18*, 551−559.
(44) Hansen, P. M.; Bhatia, V. K. l.; Harrit, N.; Oddershede, L. Expanding the optical trapping range of gold nanoparticles. *Nano Lett.* **2005**, *5*, 1937−1942.
(45) Jensen, T. R.; Malinsky, M. D.; Haynes, C. L.; Van Duyne, R. P. Nanosphere lithography: Tunable localized surface plasmon resonance spectra of silver nanoparticles. *J. Phys. Chem. B* **2000**, *104*, 10549−10556.

DOI: 10.1021/acs.nanolett.5b03833
Nano Lett. XXXX, XXX, XXX−XXX